Quantum squeezing of slow-light dark solitons via electromagnetically induced transparency

Jinzhong Zhu [1] and Guoxiang Huang [1,2,3]

[1] *State Key Laboratory of Precision Spectroscopy, East China Normal University, Shanghai 200241, China*
[2] *NYU-ECNU Joint Institute of Physics, New York University at Shanghai, Shanghai 200062, China*
[3] *Collaborative Innovation Center of Extreme Optics, Shangri University, Taiyuan 030006, China*

(Received 19 December 2021; accepted 1 March 2022; published 18 March 2022)

We consider the quantum effect of slow-light dark soliton (SLDS) in a cold atomic gas with defocusing Kerr nonlinearity via electromagnetically induced transparency (EIT). We calculate the quantum fluctuations of the SLDS by solving the relevant non-Hermitian eigenvalue problem describing the quantum fluctuations and find that only one zero mode is allowed. This is different from the quantum fluctuations of bright solitons, where two independent zero modes occur. We rigorously prove that the eigenmodes, which consist of continuous modes and the zero mode, are biorthogonal and constitute a complete biorthonormalized basis, useful for the calculation on the quantum fluctuations of the SLDS. We demonstrate that, due to the large Kerr nonlinearity contributed from the EIT effect, a significant quantum squeezing of the SLDS can be realized; the squeezing efficiency can be manipulated by the Kerr nonlinearity and the soliton's amplitude, which can be much higher than that of bright solitons. Our work contributes to efforts for developing quantum nonlinear optics and non-Hermitian physics and for possible applications in quantum information processing and precision measurements.

DOI: 10.1103/PhysRevA.105.033515

I. INTRODUCTION

Optical dark pulses, localized dips (or holes) on a homogeneous bright background, have received much attention in classical and quantum optics. Compared with bright pulses, they possess many attractive advantages, including being more stable and less sensitive to noise [1,2], which are desirable for information processing and transformation and hence they play significant roles in many research fields of physics [3–10]. One typical example of dark pulses is optical dark solitons, formed by the balance between dispersion and defocusing Kerr nonlinearity [1,2].

In recent years, much attention has been paid to the research on electromagnetically induced transparency (EIT), an important quantum interference effect typically occurring in a Λ-type three-level atomic system that interacts resonantly with two laser fields. EIT can be used to suppress resonant optical absorption, slow down group velocity, enhance Kerr nonlinearity, etc., and hence has tremendous practical applications [11,12]. Interestingly, EIT systems support slow-light solitons [13–21], which can be manipulated actively [21–23]. However, up to now most works have been mainly focused on slow-light bright solitons and limited to a semiclassical regime [24].

In this article, we investigate the quantum effect of optical dark pulses in a cold, three-level atomic gas working on the condition of EIT. By using suitable one- and two-photon detunings, a large defocusing Kerr nonlinearity and, hence, slow-light dark solitons (SLDS) can be generated in the system. The expression of the quantum fluctuations of the SLDS is obtained through solving Bogoliubov–de Gennes (BdG) equations, which are non-Hermitian eigenvalue problems describing the quantum fluctuations. We find that this eigenvalue problem allows only a single zero mode (i.e., an eigenmode with zero eigenvalue), which is different from the case of bright-soliton fluctuations where there are two independent zero modes.

Based on the above results, we rigorously prove that all eigenmodes, consisting of continuous (Goldstone) modes and the zero mode, are biorthogonal and constitute a complete bi-orthonormal basis, by which the quantum dynamics of the SLDS can be studied analytically. We demonstrate that a significant quantum squeezing of the SLDS can be realized, which originates from the large Kerr nonlinearity of the system. Moreover, the squeezing efficiency can be manipulated by the Kerr nonlinearity and the soliton amplitude; interestingly, the squeezing efficiency of the SLDS is higher than that of bright solitons. The method and results presented here are useful for developing quantum nonlinear optics and non-Hermitian physics [25–28] and may be applied to the study of Bose-Einstein condensation, quantum information processing, and precision measurements, etc.

Before preceding, we stress that, although a large number of studies on quantum optical solitons have been reported in the past years, our work is different from those studies for the following reasons.

(i) Most studies on quantum effects of optical solitons reported so far have been devoted to the bright solitons in optical fibers [29–59]. The main analytical approach used is soliton perturbation theory. Generally, perturbations on solitons have contributions from both zero modes and continuous modes, but most of these studies have considered zero modes only. Although in Refs. [37,46] continuous modes were taken into account, the completeness and orthonormality

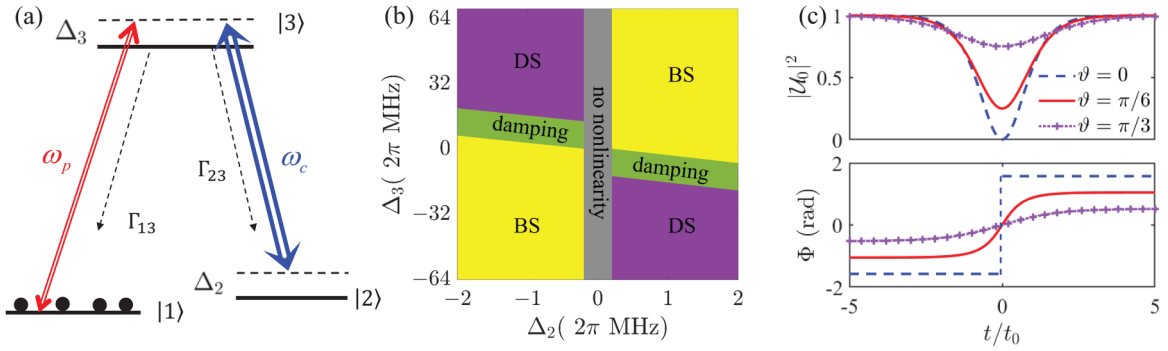

FIG. 1. (a) Excitation scheme of the EIT-based Λ-type atomic gas. Solid black dots mean that the atoms are initially prepared at the ground state $|1\rangle$. For more detail, see text. (b) Existence regions of slow-light dark and bright solitons in the plane of one-photon detuning Δ_3 and two-photon detuning Δ_2. Yellow: the region where bright solitons (BS) exist; purple: the region where dark solitons (DS) exist; green: the region where the damping is dominant over the dispersion and Kerr nonlinearity; gray: the region where Kerr nonlinearity plays no significant role. In both the green and the gray regions, no solitons exist. (c) Dimensionless dark soliton intensity (upper panels) $|\mathcal{U}_0|^2$ and phase (lower panel) Φ as functions of dimensionless time t/t_0 for different values of blackness parameter ϑ.

of the eigenmode set were not discussed [60]. In our work, all the eigenmodes are obtained, and their completeness and orthonormality are proved rigorously.

(ii) The quantum effect of dark solitons in optical fibers was investigated in Refs. [40,56]; however, the contribution of continuous modes was not considered there. In addition, the zero modes, as has been done for bright solitons [33–40], were determined by a phenomenological method (i.e., they were obtained by simply taking the derivatives of the soliton solution with respect to the free parameters in the solution). Such a method and related results obtained are uncomplete or incorrect because the zero modes obtained are generally not independent (see the discussion in Sec. III B below). Differently, in our work the eigenmodes are acquired by solving the eigenvalue problem of the perturbation, and the zero modes are determined by the requirement of the completeness and orthonormality of all the eigenmodes. The results presented in our work provide a clear way to avoid puzzles and confusion regarding the zero mode problem in previous studies [40,56,61–65] of perturbation and quantum effects of dark solitons.

(iii) At variance with Refs. [29–59], which study the quantum solitons in optical fibers, the work reported here is on the quantum effect of SLDS generated in a cold atomic gas via EIT. Our work can be taken as an extension of a recent publication [66], but it is not a simple extension because the perturbation approach of the SLDS is quite different from that of slow-light bright solitons. One of the main differences is that the SLDS have a continuous background, which makes the eigenvalue problem of the perturbation be very different from that of the slow-light bright solitons. In particular, the system allows only a single zero mode (not like the case of slow-light bright solitons where two independent zero modes occur) and the quantum squeezing of the SLDS displays behavior different from that of the slow-light bright solitons.

The remainder of the article is organized as follows. In Sec. II, we present the model under study and the quantum nonlinear Schrödinger (QNLS) equation describing the nonlinear evolution of the quantized probe laser field. In Sec. III, we diagonalize the effective Hamiltonian by expressing the quantum fluctuations of the SLDS as a superposition of the complete and biorthonormalized eigenmodes, obtained by solving the eigenvalue problem (BdG equations) of the quantum fluctuations. In Sec. IV, the quantum squeezing of the SLDS is investigated in detail. Last, Sec. V gives a summary of the main results obtained in this work.

II. MODEL AND ENVELOPE EQUATION FOR THE PROPAGATION OF THE QUANTIZED PROBE FIELD

A. Physical model

The system we consider is a cold atomic gas interacting with a probe laser field and a control laser field, forming a standard Λ-type three-level configuration [see Fig. 1(a)]. In the system, $|1\rangle$ and $|2\rangle$ are two nearly degenerate ground states, and $|3\rangle$ is an excited state with spontaneous-emission decay rates $\Gamma_{\alpha 3}$ ($\alpha = 1$ and 2) to $|1\rangle$ and $|2\rangle$, respectively. The probe field is weak and pulsed (with center angular frequency ω_p and wave number $k_p = \omega_p/c$, where c is light speed in vacuum), coupling to the transition $|1\rangle \leftrightarrow |3\rangle$; the control laser field is a strong continuous wave (with angular frequency ω_c and wave number $k_c = \omega_c/c$), coupling to the transition $|2\rangle \leftrightarrow |3\rangle$. Δ_2 and Δ_3 are two- and one-photon detunings, respectively. For suppressing the Doppler effect, both the probe and the control fields are assumed to propagate along the same (i.e., z) direction.

For simplicity, we assume the atomic gas is cigar shaped, which can be realized by filling it into a waveguide or by taking the transverse distribution of the probe field to be large enough so that the diffraction effect can be neglected. Thus, one can use a reduced $(1+1)$-dimensional model to describe the probe-field propagation, with the total electric field given by $\hat{\mathbf{E}}(z,t) = \mathbf{E}_c(z,t) + \hat{\mathbf{E}}_p(z,t)$. Here, $\mathbf{E}_c(z,t) \equiv \mathbf{e}_c \mathcal{E}_c(z,t) e^{i(k_c z - \omega_c t)} + \text{c.c.}$ and $\hat{\mathbf{E}}_p(z,t) \equiv \mathbf{e}_p \mathcal{E}_p \hat{E}_p(z,t) e^{i(k_p z - \omega_p t)} + \text{H.c.}$ are respectively the quantized probe and c-number control fields, with c.c. (H.c.) representing the conjugate (Hermitian conjugate); $\mathbf{e}_c$ and $\mathcal{E}_c$ are respectively the unit polarization vector and the amplitude of the control field; $\mathbf{e}_p$ and $\mathcal{E}_p \equiv \sqrt{\hbar\omega_p/(2\varepsilon_0 V)}$ (V is quantized volume) are respectively the unit polarization vector and the single-photon amplitude of the probe field. $\hat{E}_p(z,t)$ is a

slowly-varying annihilation operator of probe photons, obeying the commutation relation $[\hat{E}_p(z,t), \hat{E}_p^\dagger(z',t)] = L\delta(z'-z)$, with L being the quantization length along the z axis.

Under electric-dipole and paraxial approximations, the system Hamiltonian is given by $\hat{H} = \int dz\, [-\frac{\hbar c}{L}\hat{E}_p^\dagger(i\frac{\partial}{\partial z})\hat{E}_p - \frac{\hbar N}{L}(\sum_{\alpha=2,3}\Delta_\alpha \hat{S}_{\alpha\alpha} + g_p\hat{S}_{31}^\dagger\hat{E}_p + \Omega_c\hat{S}_{32}^\dagger + \text{H.c.})]$. Here N is the total atomic number of the system; $\hat{S}_{\alpha\beta}(z,t) = \hat{\sigma}_{\beta\alpha}\, e^{i[(k_\beta-k_\alpha)z-(\omega_\beta-\omega_\alpha+\Delta_\beta-\Delta_\alpha)t]}$ ($\alpha, \beta = 1$, 2, and 3) are atomic transition operators; $\Omega_c = (\mathbf{e}_c\cdot\mathbf{p}_{32})\mathcal{E}_c/\hbar$ is the half Rabi frequency of the control field; $g_p = (\mathbf{e}_p\cdot\mathbf{p}_{31})\mathcal{E}_p/\hbar$ is the single-photon half Rabi frequency of the probe field; $\mathbf{p}_{\alpha\beta}$ is the electric dipole matrix element associated with the transition from $|\beta\rangle$ to $|\alpha\rangle$; and the detunings are defined by $\Delta_2 = \omega_p - \omega_c - (\omega_2-\omega_1)$ and $\Delta_3 = \omega_p - (\omega_3-\omega_1)$.

The dynamics of the system is governed by the Heisenberg-Langevin and the Maxwell (HLM) equations, given by

$$\frac{\partial}{\partial t}\hat{S}_{\alpha\beta} = \frac{1}{i\hbar}[\hat{S}_{\alpha\beta}, \hat{H}] - \hat{\mathcal{L}}(\hat{S}_{\alpha\beta}) + \hat{F}_{\alpha\beta}, \tag{1a}$$

$$i\left(\frac{\partial}{\partial z} + \frac{1}{c}\frac{\partial}{\partial t}\right)\hat{E}_p + \frac{g_p^* N}{c}\hat{S}_{31} = 0, \tag{1b}$$

where $\hat{\mathcal{L}}(\hat{S}_{\alpha\beta})$ is the 3×3 relaxation matrix including the atomic decay rates of the spontaneous emission and dephasing, $\hat{F}_{\alpha\beta}$ are δ-correlated Langevin noise operators introduced to preserve the Heisenberg commutation relations for the operators of the atoms and the probe field. Explicit expressions of Eq. (1a) are presented in Appendix A.

The model described above can be realized by many atomic systems. One of the candidates is the laser-cooled alkali-metal ^{87}Rb gas, which is used below, with the levels chosen to be $|1\rangle = |5^2S_{1/2}, F=1, m_F=1\rangle$, $|2\rangle = |5^2S_{1/2}, F=2, m_F=1\rangle$, and $|3\rangle = |5^2P_{3/2}, F=2, m_F=1\rangle$, with $\Gamma_{13} = \Gamma_{23} \approx 2\pi \times 3$ MHz [67].

B. Nonlinear envelope equation and the existence region of dark solitons in parameter space

To understand the quantum dynamics of the system, we need to solve the nonlinearly coupled equations, Eqs. (1a) and (1b), which have many degrees of freedom of atoms and photons and thus are not easy to approach. A convenient way is to reduce such equations to an effective one by eliminating the atomic degrees of freedom under some approximations, which has been recently used in the study of polaritons in atomic gases [68–70]. Similar to Ref. [66], by employing the perturbation expansion under weak-dispersion and weak-nonlinearity approximations, one can obtain the following QNLS equation:

$$i\left[\left(\frac{\partial}{\partial z} + \frac{1}{V_g}\frac{\partial}{\partial t}\right) + \text{Im}(K_0)\right]\hat{E}_p - \frac{K_2}{2}\frac{\partial^2}{\partial t^2}\hat{E}_p + W|g_p|^2\hat{E}_p^\dagger\hat{E}_p\hat{E}_p - i\hat{\mathcal{F}}_p e^{-i\tilde{K}_0 z} = 0, \tag{2}$$

which describes the nonlinear evolution of the probe-field envelope $\hat{E}_p$. Here, $K_j \equiv (\partial^j K/\partial\omega^j)^{-1}|_{\omega=0}$ ($j = 0$, 1, and 2), with $K = K(\omega)$ being the linear dispersion relation, $V_g \equiv 1/K_1$ being the group velocity, and K_2 being the coefficient of the group-velocity dispersion; W is the coefficient of third-order Kerr nonlinearity, which is proportional to the third-order nonlinear optical susceptibility $\chi_p^{(3)}$; and $\hat{\mathcal{F}}_p(z,t)$ is the δ-correlated induced Langevin noise operator. For explicit expressions of $K(\omega)$, W, and $\hat{\mathcal{F}}_p(z,t)$, see Appendix B. Note that, in general, the coefficients in Eq. (2) depend on ω (i.e., the sideband frequency of the probe pulse). Because we are interested in the propagation of the probe pulse with the center frequency ω_p, the coefficients in Eq. (2) are estimated at $\omega = 0$. In this situation, these coefficients (K_2, W, etc.) are functions of the one- and two-photon detunings (i.e., Δ_3 and Δ_2) and other system parameters (see Ref. [66]).

The coefficients of Eq. (2) are generally complex due to the near-resonant character of the system. However, under the condition of EIT (i.e., $|\Omega_c|^2 \gg \gamma_{21}\gamma_{31}$), the imaginary parts of these coefficients are much smaller than their real parts and hence can be neglected. Depending on the sign of W/K_2, in the case of classical limit and negligible noise, Eq. (2) admits dark (bright) soliton solutions for $W/K_2 > 0$ ($W/K_2 < 0$).

Figure 1(b) shows the existence regions of dark and bright solitons in the parameter space with Δ_3 and Δ_2 as two coordinates. In the figure, the purple region "DS" (yellow region "BS") is the one where dark (bright) solitons exist. The green region indicated by "damping" is the one where the damping of the probe field is dominant over the group-velocity dispersion and the Kerr nonlinearity; the gray region indicated by "no nonlinearity" means that in this domain the Kerr nonlinearity plays no significant role. Thus, in both the green and the gray regions, the system does not support solitons [24]. When plotting the figure, we have taken $\Gamma_{13} = \Gamma_{23} \approx 2\pi \times 3$ MHz, $\mathcal{N}_a$ (atomic density) $= 8.8 \times 10^{11}$ cm^{-3}, $|g_p|^2N/c = 2.4 \times 10^{10}$ cm^{-1} s^{-1}, $\Omega_c = 2\pi \times 42$ MHz, and t_0 (the time duration of the probe pulse) $= 5.5 \times 10^{-8}$ s.

Since the atomic gas is nearly resonant with the probe and control fields and works under the condition of EIT, the system can possess a large Kerr nonlinearity. As an example, by taking $\Delta_2 = -2\pi \times 1.6$ MHz and $\Delta_3 = 2\pi \times 64$ MHz, and using the formulas for the linear dispersion relation K and the Kerr coefficient W given in Appendix B, we obtain $K_1 \approx 3.08 \times 10^{-7}$ cm^{-1} s, $K_2 \approx 3.19 \times 10^{-15}$ cm^{-1} s^2, and $W \approx 8.20 \times 10^{-17}$ cm^{-1} s^2. Thus, we have

$$\chi_p^{(3)} = \frac{2c|\mathbf{e}_p\cdot\mathbf{p}_{31}|^2}{\hbar^2\omega_p}W \approx 1.20 \times 10^{-10}\,\text{m}^2\,\text{V}^{-2}. \tag{3}$$

Because $\chi_p^{(3)}$ is proportional to Δ_2, so nonzero two-photon detuning (i.e., $\Delta_2 \neq 0$) is necessary to obtain the large Kerr nonlinearity. Such a Kerr nonlinearity, which is more than 10 orders of magnitude larger than that of conventional optical media (such as optical fibers) [1], is the main reason why optical solitons can form at very low-light levels in EIT-based atomic gases [13–24].

Note that even for the large Kerr nonlinearity given above, the perturbation expansion used for deriving the QNLS equation (2) can still be applied. The reasons are the following. In our consideration the light intensity of the probe pulse is small, and its time duration is large (which means that its dispersion is weak). Thus, the perturbation expansion is obtained under weak-dispersion and weak-nonlinearity approximations. In fact, similar perturbation expansion was used in Refs. [13–24].

After neglecting the imaginary parts of K_1, K_2, and W, Eq. (2) can be written as the dimensionless form $i\frac{\partial}{\partial s}\hat{U} + \frac{\partial^2}{\partial\tau^2}\hat{U} - 2g\hat{U}^\dagger\hat{U}\hat{U} = -2i\nu\hat{U} + i\hat{f}_p$, with $\hat{U} = \hat{E}_p/\sqrt{n_0}$ ($n_0 \gg 1$ is the typical mean photon number in the probe field [71]), $s = z/(2L_{\rm disp})$, $\tau = (t - z/V_g)/t_0$, $\hat{f}_p = 2L_{\rm disp}\hat{\mathcal{F}}_p e^{-iK_0 z}$, $\nu = L_{\rm disp}/L_{\rm abs}$, and $g = L_{\rm disp}/L_{\rm nln}$ (the dimensionless parameter characterizes the magnitude of the Kerr nonlinearity). Here, $L_{\rm disp} \equiv t_0^2/|K_2|$, $L_{\rm nln} \equiv [n_0|g_p|^2|W|]^{-1}$, and $L_{\rm abs} \equiv 1/{\rm Im}(K_0)$ are the typical dispersion length, nonlinearity length, and absorption length of the probe field, respectively.

Due to the EIT effect and the ultracold environment, the Langevin noise operators make no contribution to the normally ordered correlation functions of system operators [72,73], also the dimensionless absorption coefficient $\nu \approx 1.69 \times 10^{-2} \ll 1$. Taking into account these facts and making the transformation $\hat{U} = \hat{\tilde{U}}e^{-i\mu s}$, we obtain the reduced QNLS equation

$$i\frac{\partial}{\partial s}\hat{\tilde{U}} = -\frac{\partial^2}{\partial\tau^2}\hat{\tilde{U}} + 2g\hat{\tilde{U}}^\dagger\hat{\tilde{U}}\hat{\tilde{U}} - \mu\hat{\tilde{U}}, \tag{4}$$

with the parameter μ being the "chemical potential" to be specified in the next section. The *effective* Hamiltonian for the system described by the QNLS equation (4) reads

$$\hat{H}_{\rm eff} = \int_{-\infty}^{+\infty} d\tau\hat{\tilde{U}}^\dagger\left(-\frac{\partial^2}{\partial\tau^2} - \mu - g\hat{\tilde{U}}^\dagger\hat{\tilde{U}}\right)\hat{\tilde{U}}. \tag{5}$$

III. COMPLETE AND BIORTHONORMAL SET OF THE EIGENMODES FOR THE QUANTUM FLUCTUATIONS OF SLOW-LIGHT DARK SOLITONS

A. Slow-light dark solitons

Our main aim is to investigate the quantum fluctuations from classical dark solitons. As a first step, we consider the classical limit of the system, which is valid when the probe field contains a large photon number. In this case, the operator $\hat{\tilde{U}}$ can be approximated by a c-number function $\mathcal{U}_0$. Then the reduced QNLS equation (4) becomes a classical NLS equation of the form $i\partial\mathcal{U}_0/\partial s + \partial^2\mathcal{U}_0/\partial\tau^2 - 2g|\mathcal{U}_0|^2\mathcal{U}_0 + \mu\mathcal{U}_0 = 0$. When working in the "DS" region of Fig. 2(b), this equation admits the fundamental dark-soliton solution

$$\mathcal{U}_0(s,\tau) = \mathcal{A}\sqrt{g}(\cos\vartheta\tanh\sigma + i\sin\vartheta)e^{i\theta_0}, \tag{6}$$

with $\sigma = \mathcal{A}g\cos\vartheta(\tau - \tau_0 - 2\mathcal{A}g\sin\vartheta s)$ and $\mu = 2\mathcal{A}^2g^2$. Here, $\mathcal{A}$ and θ_0 are constants characterizing the amplitude and the overall phase of the soliton; ϑ ($0 \leqslant \vartheta \leqslant \pi/2$) is a constant characterizing the dark-soliton blackness, defined by $\mathcal{A}^2g\cos^2\vartheta$ (i.e., the difference between the minimum of the soliton intensity and the background intensity $\mathcal{A}^2g$); and the "momentum" and the initial "position" of the soliton are given by $2\mathcal{A}g\sin\vartheta$ and τ_0, respectively. The soliton for the special case $\vartheta = 0$ is called the black soliton; in the general case ($\vartheta \neq 0$), it is called the dark (or gray) soliton. Figure 1(c) shows the profile of the dimensionless dark-soliton intensity $|\mathcal{U}_0|^2$ (upper part) and phase $\Phi \equiv \arctan(\cos\vartheta\tanh\sigma/\sin\vartheta)$ (lower part) with different values of the blackness parameter ϑ. When plotting the figure, we have taken $\mathcal{A} = g = 1$, and hence the background intensity of the dark soliton is $\mathcal{A}^2g = 1$.

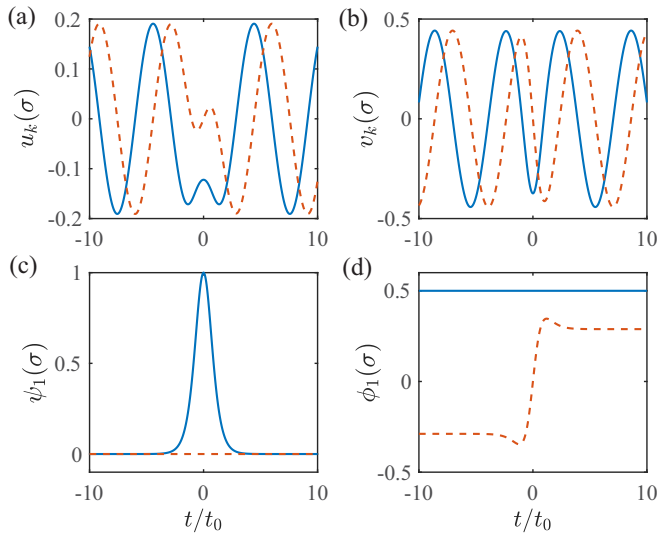

FIG. 2. (a)–(d) Eigenmode functions $u_k(\sigma)$, $v_k(\sigma)$, $\psi_1(\sigma)$, and $\phi_1(\sigma)$, respectively, plotted with wave number $k = 1$ and blackness parameter $\vartheta = \pi/6$. The solid (dashed) line represents the relevant real (imaginary) part.

By using the physical parameters given in Sec. II B, we can estimate the propagation velocity of the dark soliton, given by

$$V_{\rm sol} = V_g + \frac{\mathcal{A}gt_0\sin\vartheta}{L_{\rm disp}} \approx 1.08 \times 10^{-4}c, \tag{7}$$

with $\mathcal{A} = 1$, $t_0 = 5.5 \times 10^{-8}$ s, and $\vartheta = \pi/2$. We see that the soliton velocity is much smaller than c (i.e., it indeed is a SLDS), which is due to the EIT effect induced by the control field.

B. Eigenmodes of the quantum fluctuations and their biorthogonality and completeness

1. Eigenvalue problem of the quantum fluctuations

Now we consider the quantum correction of the SLDS solution (6). We assume the mean photon number n_0 in the probe field is much larger than 1, the quantum fluctuations of the SLDS are weak, and hence we can take the Bogoliubov decomposition

$$\hat{\tilde{U}}(s,\tau) = \mathcal{U}_0(\tau) + \hat{U}_1(s,\tau), \tag{8}$$

where $\mathcal{U}_0(\tau) = \mathcal{U}_0(0,\tau)$ is a classical SLDS background for $s = 0$, and $\hat{U}_1$ is the annihilation operator of photons representing the quantum fluctuations (perturbations) on the SLDS background $\mathcal{U}_0(\tau)$, satisfying the commutation relation $[\hat{U}_1(s,\tau), \hat{U}_1^\dagger(s,\tau')] = \delta(\tau - \tau')$. For the convenience of the following calculations, we introduce $\hat{w} \equiv \hat{U}_1/(\sqrt{\mathcal{A}g\cos\vartheta})$, which satisfies $[\hat{w}(s,\sigma), \hat{w}^\dagger(s,\sigma')] = \delta(\sigma - \sigma')$.

Substituting the Bogoliubov decomposition (8) into the reduced QNLS equation (4) and neglecting the high-order terms of $\hat{U}_1$, we obtain the following equation for $\hat{w}$ and $\hat{w}^\dagger$:

$$i\frac{\partial}{\partial s}\begin{pmatrix}\hat{w}\\ \hat{w}^\dagger\end{pmatrix} - \mathcal{A}^2g^2\cos^2\vartheta\,\hat{\mathcal{L}}\begin{pmatrix}\hat{w}\\ \hat{w}^\dagger\end{pmatrix} = 0, \tag{9}$$

where $\hat{\mathcal{L}}$ is a linear matrix operator, defined by

$$\hat{\mathcal{L}} = \begin{pmatrix} \mathcal{M} + 2i\gamma\frac{\partial}{\partial\sigma} & 2\mathcal{N} \\ -2\mathcal{N}^* & -\mathcal{M} + 2i\gamma\frac{\partial}{\partial\sigma} \end{pmatrix}, \tag{10}$$

with $\mathcal{M} = -\frac{\partial}{\partial\sigma^2} + 4\tanh^2\sigma - 2 + 2\gamma^2$, $\mathcal{N} = (\tanh\sigma + i\gamma)^2$, and $\gamma = \tan\vartheta$.

To solve Eq. (9) for all possible quantum fluctuations, the key is to find the eigenmodes of the operator $\hat{\mathcal{L}}$ and constitute an orthogonal and complete set of them. The difficulty of success for this depends on the property of $\hat{\mathcal{L}}$. Obviously, $\hat{\mathcal{L}}$ is *non-Hermitian*; its adjoint operator is given by

$$\hat{\mathcal{L}}^\dagger = \sigma_3\hat{\mathcal{L}}\sigma_3 = \begin{pmatrix} \mathcal{M} + 2i\gamma\frac{\partial}{\partial\sigma} & -2\mathcal{N} \\ 2\mathcal{N}^* & -\mathcal{M} + 2i\gamma\frac{\partial}{\partial\sigma} \end{pmatrix}, \tag{11}$$

where $\sigma_3 = \left(\begin{smallmatrix} 1 & 0 \\ 0 & -1 \end{smallmatrix}\right)$ is a Pauli matrix. Although $\hat{\mathcal{L}}$ is not Hermitian, i.e., $\hat{\mathcal{L}}^\dagger \neq \hat{\mathcal{L}}$, it is *pseudo-Hermitian* due to the property $\hat{\mathcal{L}}^\dagger = \sigma_3\hat{\mathcal{L}}\sigma_3$. It is known that such a pseudo-Hermitian operator possesses real eigenvalues, and it is possible to get the eigenmodes of $\hat{\mathcal{L}}$ and $\hat{\mathcal{L}}^\dagger$, which can be complete and biorthonormal in the mutually dual-function spaces of $\hat{\mathcal{L}}$ and $\hat{\mathcal{L}}^\dagger$ [25,27].

To get the eigenmodes explicitly, we use the Bogoliubov transformation to expand the quantum fluctuations $\hat{w}$ as

$$\hat{w}(s,\sigma) = \sum_n [u_n(\sigma)\hat{a}_n(s) + v_n^*(\sigma)\hat{a}_n^\dagger(s)] + \int dk\,[u_k(\sigma)\hat{a}_k(s) + v_k^*(\sigma)\hat{a}_k^\dagger(s)]. \tag{12}$$

Here the indices n and k are quantum numbers denoting respectively the discrete and continuous modes; $\hat{a}_n(s)$ and $\hat{a}_k(s)$ are respectively annihilation operators of photons for the discrete and continuous modes, satisfying respectively the commutation relations $[\hat{a}_n(s), \hat{a}_m^\dagger(s)] = \delta_{mn}$ and $[\hat{a}_k(s), \hat{a}_{k'}^\dagger(s)] = \delta(k-k')$; $u_n(\sigma)$ and $v_n(\sigma)$ are mode functions for the discrete spectra; and $u_k(\sigma)$ and $v_k(\sigma)$ are mode functions for the continuous spectra.

Assuming $\hat{a}_j(s) = \hat{a}_j(0)e^{-iE_j\mathcal{A}^2g^2\cos^2\vartheta\, s}$, and substituting it into Eq. (9), we obtain the eigenvalue equations (i.e., BdG equations)

$$\hat{\mathcal{L}}\,|\Psi_j(\sigma)\rangle = E_j|\Psi_j(\sigma)\rangle. \tag{13}$$

Here, for simplicity, we have used the index j to denote both the discrete (for $j = n$) and the continuous (for $j = k$) spectra. The eigenvectors $|\Psi_j(\sigma)\rangle \equiv [u_j(\sigma), v_j(\sigma)]^T$, with symbol "$T$" representing transpose.

Note that the eigenmodes of the operator $\hat{\mathcal{L}}$ form a function space V_L, which is, however, not a Hilbert space because $\hat{\mathcal{L}}$ is not Hermitian. Following the standard method [25,27,74–76], we consider the dual space of $\hat{\mathcal{L}}$, i.e., the function space $V_{L^\dagger}$ of the operator $\hat{\mathcal{L}}^\dagger$. The eigenvalue problem of $\hat{\mathcal{L}}^\dagger$ reads

$$\hat{\mathcal{L}}^\dagger|\Phi_j(\sigma)\rangle = E_j^*|\Phi_j(\sigma)\rangle = E_j|\Phi_j(\sigma)\rangle \tag{14}$$

because E_j is real. The above equation is usually written in the form $\langle\Phi_j|\hat{\mathcal{L}} = E_j\langle\Phi_j|$ [25]. It is easy to show that $|\Phi_j(\sigma)\rangle = \sigma_3|\Psi_j(\sigma)\rangle$.

With the eigenmodes of the two mutually dual-function spaces V_L and $V_{L^\dagger}$, we can define the product between the right vectors $\{|\Psi_j\rangle\}$ and the left vectors $\{\langle\Phi_j|\}$:

$$\langle\Phi_j|\Psi_l\rangle = \int_{-\infty}^{\infty} d\sigma\,\langle\Phi_j(\sigma)|\Psi_l(\sigma)\rangle. \tag{15}$$

It can be shown that $\{|\Psi_j\rangle\}$ and $\{\langle\Phi_j|\}$ are biorthogonal and can be made to be normalized, i.e.,

$$\langle\Phi_j(\sigma)|\Psi_l(\sigma)\rangle = \delta_{jl}. \tag{16}$$

To implement the perturbation calculation on the quantum fluctuations of the SLDS, one needs the eigenmodes in the dual spaces not only to be biorthonormalized but also to span a complete set, so that any possible quantum fluctuations can be expanded as their linear superposition. However, the proof of the completeness for such biorthogonal eigenmodes is usually not an easy problem. If all the eigenmodes (especially the independent zero modes) are found, the completeness relationship reads

$$\sum_n |\Phi_n(\sigma)\rangle\langle\Psi_n(\sigma')| + \int_{-\infty}^{+\infty} dk|\Phi_k(\sigma)\rangle\langle\Psi_k(\sigma')| = I\delta(\sigma-\sigma'), \tag{17}$$

with I being the 2×2 unit matrix.

2. *Eigenmode solutions and their biorthogonality and completeness*

The eigenmodes for the continuum spectrum (i.e., Goldstone bosons) of the present eigenvalue problem [i.e., the BdG equations (13)] can be found in a manner similar to that of Refs. [77,78]. We obtain the solutions

$$|\Psi_k(\sigma)\rangle = \begin{pmatrix} u_k(\sigma) \\ v_k(\sigma) \end{pmatrix}, \tag{18a}$$

$$|\Phi_k(\sigma)\rangle = \sigma_3|\Psi_k(\sigma)\rangle = \begin{pmatrix} u_k(\sigma) \\ -v_k(\sigma) \end{pmatrix}, \tag{18b}$$

where the eigenvalues and eigenfunctions are given by

$$E_k^{(\pm)} = |k|[-2\gamma \pm \sqrt{k^2 + 4(1+\gamma^2)}], \tag{19a}$$

$$u_k(\sigma) = \frac{e^{ik\sigma}\left\{\tanh\sigma + \frac{i}{2}[\mathcal{D}_\pm(k) - k]\right\}^2}{\sqrt{2\pi|k|\nu(k)}\mathcal{D}_\pm(k)}, \tag{19b}$$

$$v_k(\sigma) = \frac{e^{ik\sigma}\left\{\tanh\sigma - \frac{i}{2}[\mathcal{D}_\pm(k) + k]\right\}^2}{\sqrt{2\pi|k|\nu(k)}\mathcal{D}_\pm(k)}, \tag{19c}$$

with $\mathcal{D}_\pm(k) = -2\gamma \pm \nu(k)$ and $\nu(k) = \sqrt{k^2 + 4(1+\gamma^2)}$. Note that the eigenmodes corresponding to the eigenvalue $E_k^{(-)}$ are nonphysical and hence must be excluded. The reason is due to the fact $\lim_{k\to\infty} E_k^{(-)} = -\infty$; with such an eigenvalue, the energy has no lower bound, which makes the system collapse.

The continuum eigenmode set $\{|\Psi_k(\sigma)\rangle\}$ and $\{|\Phi_k(\sigma)\rangle\}$ is not enough to constitute a complete biorthonormal basis. In fact, the operators $\hat{\mathcal{L}}$ and $\hat{\mathcal{L}}^\dagger$ allow discrete eigenmodes with zero eigenvalues, i.e., zero modes, satisfying the equations

$$\hat{\mathcal{L}}|\Psi_n(\sigma)\rangle = 0,\ |\Psi_n(\sigma)\rangle = \begin{pmatrix} u_n(\sigma) \\ v_n(\sigma) \end{pmatrix}, \tag{20a}$$

$$\hat{\mathcal{L}}^\dagger|\Phi_n(\sigma)\rangle = 0,\ |\Phi_n(\sigma)\rangle = \sigma_3|\Psi_n(\sigma)\rangle, \tag{20b}$$

$n = 1, 2, \ldots$

Since a linear superposition of multiple zero modes is also a zero mode, in general, one can get infinite many zero modes. How to choose these zero modes? The criteria for the choice of the zero modes are the following: (i) they must be independent each other; and (ii) the set consisting of the continuous modes given in Eq. (18) and the zero modes given in Eqs. (20) should constitute a complete and biorthonormal basis, which is necessary for providing an expansion basis to express any quantum fluctuation of the soliton.

Based on such criteria, we find that the system supports only a single zero mode, given by

$$|\Psi_1(\sigma)\rangle = \begin{pmatrix} u_1(\sigma) \\ v_1(\sigma) \end{pmatrix}, \tag{21a}$$

$$|\Phi_1(\sigma)\rangle = \sigma_3|\Psi_1(\sigma)\rangle = \begin{pmatrix} u_1(\sigma) \\ -v_1(\sigma) \end{pmatrix}, \tag{21b}$$

with

$$u_1(\sigma) = \frac{2\mathrm{sech}^2\sigma + i\gamma\tan\sigma + i\gamma\sigma\,\mathrm{sech}^2\sigma + 1}{2\sqrt{2}}, \tag{22a}$$

$$v_1(\sigma) = \frac{2\mathrm{sech}^2\sigma + i\gamma\tan\sigma + i\gamma\sigma\,\mathrm{sech}^2\sigma - 1}{2\sqrt{2}}. \tag{22b}$$

It can be rigorously proved that, for our present system, the eigenmode set $\{|\Psi_k(\sigma)\rangle, |\Psi_1(\sigma)\rangle\}$ and $\{|\Phi_k(\sigma)\rangle, |\Phi_1(\sigma)\rangle\}$ given by Eqs. (19) (taking only the $E_k^{(+)}$ mode) and (22) is not only biorthonormal, but also complete, satisfying Eqs. (16) and (17). A detailed proof for this is presented in Appendix C. When $\gamma = 0$ (i.e., for the special case of black solitons), these results are consistent with those obtained in previous studies [79,80].

Taking the transformations

$$u_1 = \frac{1}{\sqrt{2}}(\psi_1 + \phi_1), \tag{23a}$$

$$v_1^* = \frac{1}{\sqrt{2}}(\psi_1 - \phi_1), \tag{23b}$$

$$\hat{Q}_1 = \frac{1}{\sqrt{2}}(\hat{a}_1 + \hat{a}_1^\dagger), \tag{23c}$$

$$\hat{P}_1 = \frac{1}{\sqrt{2}i}(\hat{a}_1 - \hat{a}_1^\dagger), \tag{23d}$$

where $\hat{Q}_1$ and $\hat{P}_1$ are "coordinate" operators and "momentum" operators, satisfying the commutation relations $[\hat{Q}_1, \hat{Q}_1] = [\hat{P}_1, \hat{P}_1] = 0$ and $[\hat{Q}_1, \hat{P}_1] = i$, we obtain the general expression of the quantum fluctuations of the SLDS in the following form:

$$\hat{w} = \psi_1(\sigma)\hat{Q}_1(s) + i\phi_1(\sigma)\hat{P}_1(s), + \int_{-\infty}^{+\infty} dk[u_k(\sigma)\hat{a}_k(s) + v_k^*(\sigma)\hat{a}_k^\dagger(s)]. \tag{24}$$

Based on this expression, the effective Hamiltonian (5) is diagonalized to be

$$\hat{H}_{\mathrm{eff}} = \mathcal{A}^2 g^2 \cos^2\vartheta \times \left[\frac{1}{2}P_1^2(s) + \int_{-\infty}^{+\infty} dk E_k^{(+)}\hat{a}_k^\dagger(s)\hat{a}_k(s)\right], \tag{25}$$

with $\psi_1(\sigma) = \mathrm{sech}^2\sigma$ and $\phi_1(\sigma) = (i\gamma\tan\sigma + i\gamma\sigma\,\mathrm{sech}^2\sigma + 1)/2$. Figures 2(a)–2(d) show the profiles of $\psi_1(\sigma)$, $\phi_1(\sigma)$, $u_k(\sigma)$, and $v_k(\sigma)$ as functions of σ, respectively. The term $P_1^2/2$ in Eq. (25) is contributed by the zero mode. We see that the zero mode behaves like a free particle and its mass is positive, which means that the SLDS is quite stable when the quantum fluctuations exist in the system.

We must stress that the zero mode given by Eq. (21) is not corresponding to a Goldstone boson, though its origin has some similarities to that of Goldstone bosons [81]. The zero mode is a discrete eigenmode of the system. It is different from the Goldstone bosons described by the continuous eigenmodes, which also have a zero frequency as lower bound of the continuum of frequency. In fact, the appearance of the zero mode is due to the existence of the SLDS, which are inhomogeneous in space. If the classical background $\mathcal{U}_0$ in the Bogoliubov decomposition (8) is a constant, the zero mode will disappear. For a similar discussion on relativistic quantum field theory, see Ref. [82].

IV. QUANTUM SQUEEZING OF SLOW-LIGHT DARK SOLITONS

A. Quantum dynamics of slow-light dark solitons

Based on the diagonalized effective Hamiltonian (25), it is easy to study the quantum dynamics of the SLDS. The Heisenberg equations of motion for $\hat{Q}_1(s)$, $\hat{P}_1(s)$, and $\hat{a}_k(s)$ read

$$\frac{\partial}{\partial s}\hat{Q}_1(s) - \mathcal{A}^2 g^2\cos^2\vartheta\hat{P}_1(s) = 0, \tag{26a}$$

$$\frac{\partial}{\partial s}\hat{P}_1(s) = 0, \tag{26b}$$

$$i\frac{\partial}{\partial s}\hat{a}_k(s) - \mathcal{A}^2 g^2\cos^2\vartheta E_k^{(+)}\hat{a}_k(s) = 0. \tag{26c}$$

The exact solutions of these equations can be obtained, given by

$$\hat{Q}_1(s) = \hat{Q}_1(0) + \mathcal{A}^2 g^2\cos^2\vartheta\hat{P}_1(0)s, \tag{27a}$$

$$\hat{P}_1(s) = \hat{P}_1(0), \tag{27b}$$

$$\hat{a}_k(s) = \hat{a}_k(0)e^{-i\mathcal{A}^2 g^2\cos^2\vartheta E_k^{(+)}s}, \tag{27c}$$

where $\hat{Q}_1(0)$, $\hat{P}_1(0)$, and $\hat{a}_k(0)$ are the values of $\hat{Q}_1(s)$, $\hat{P}_1(s)$, and $\hat{a}_k(s)$ at $s = 0$, respectively. From Eqs. (26) and their solutions (27), we have the following conclusions.

(i) The quantum fluctuations contributed by the zero mode display specific characters. The momentum operator $\hat{P}_1$ remains unchanged during propagation (i.e., the momentum of the SLDS is conserved); while the evolution of the position operator $\hat{Q}_1$ depends on $\hat{P}_1(0)$, the value of the momentum operator $\hat{P}_1$ at $s = 0$. Such a correlation between $\hat{Q}_1$ and $\hat{P}_1$ leads to a position spreading of the SLDS, contributed by the Kerr nonlinearity (characterized by the nonlinear parameter g). However, photon-number and phase fluctuations are not predicted here, different from the case of bright solitons [66,83,84].

(ii) The quantum fluctuation of the continuum modes (characterized by the quantum number k) has only a simple

effect, i.e., a phase shift to the same mode caused by the Kerr nonlinearity.

From formulas (6) and (12), we can get the approximate expression of the quantized probe field by using the renormalization technique [85], given by

$$\hat{\tilde{U}}(s,\sigma) \approx \mathcal{A}\sqrt{g}\left[\cos\vartheta \tanh\left(\sigma + \frac{\hat{Q}_1}{\sqrt{g}}\right) + i\sin\vartheta\right] e^{i\theta_0 + i\frac{\hat{P}_1\sigma}{\mathcal{A}\sqrt{g}}}. \tag{28}$$

One can see clearly that the quantum fluctuations of the SLDS are mainly contributed by the zero mode, which propagates together with the soliton; the conjugated operator pair $\hat{Q}_1$ and $\hat{P}_1$ describe the position and momentum fluctuations, respectively. The reason for no fluctuation of particle number (amplitude) and phase is as follows. In our approach, the SLDS has an infinite large background [i.e., it contains a very large (infinite) photon number], and hence no phase diffusion occurs in the presence of perturbations. If, however, the system has a finite size (e.g., when there is an external potential $V_{\rm ext}$ acting on the system, the photon number in the soliton will be finite), a phase diffusion of the soliton will happen.

With these results, we can give a numerical estimation on the quantum fluctuations of the SLDS. Let $|\Psi\rangle = |n_0, n_1, n_c\rangle$ denote the quantum state with n_0 photons in the SLDS; n_1 photons in the zero mode, and n_c photons in the continuous modes. We assume that, at the entrance of the system ($s = 0$), the quantum state of the probe field is in the "vacuum" state $|\Psi_0\rangle = |n_0, 0, 0\rangle$ (i.e., the probe field has no quantum fluctuation). Based on the analytical result (27), we obtain $\langle\hat{Q}_1(s)\rangle = \langle\hat{P}_1(s)\rangle = 0$ and $\langle\hat{Q}_1^2(0)\rangle = \langle\hat{P}_1^2(0)\rangle = 1/2$; the variances (mean-squared derivations) as functions of s are given by

$$\langle\hat{P}_1^2(s)\rangle = \tfrac{1}{2}, \tag{29}$$

$$\langle\hat{Q}_1^2(s)\rangle = \tfrac{1}{2}(1 + \mathcal{A}^4 g^4 \cos^4\vartheta\, s^2). \tag{30}$$

Here $\langle\cdots\rangle \equiv \langle\Psi_0|\cdots|\Psi_0\rangle$. One sees that the variance of the position fluctuation is propagation dependent, while the variance of the momentum fluctuation is a constant during propagation.

B. Quantum squeezing of slow-light dark solitons

In recent years, a multitude of studies have been dedicated to quantum squeezing [86,87]. In particular, many efforts have focused on the quantum squeezing of light, which has important applications, especially for quantum precision measurements (e.g., the detection of gravitational waves) [88]. The results obtained above can be exploited to investigate the quantum squeezing of the SLDS, which can be measured using a homodyne detection method [33,38]. In comparison with the zero mode, the quantum fluctuations from the continuous modes are much weaker and hence are neglected in the following calculation.

The quantum squeezing of the SLDS may be described by the quadrature operators at the angle θ related to the operator

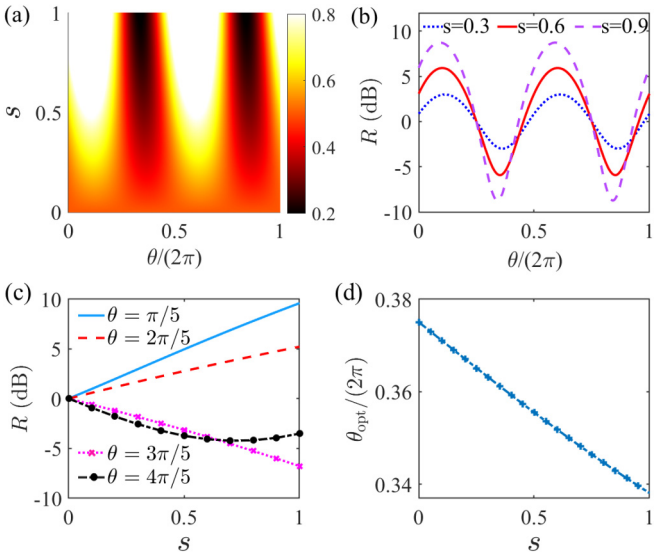

FIG. 3. (a) Quadrature variance $\langle\hat{X}_\theta^2\rangle$ of the SLDS as a function of $s = z/(2L_{\rm disp})$ (dispersion length $L_{\rm disp} = 0.95\,{\rm cm}$) and $\theta/(2\pi)$. Different colors shown in the color bar denote different magnitudes of $\langle\hat{X}_\theta^2\rangle$. The quadrature variance in the black domains is much smaller than its vacuum value, indicating that the SLDS displays larger quadrature squeezing. (b) Squeezing ratio R (unit dB) versus detection angle θ with $s = 0.3$, 0.6, and 0.9, plotted by dotted blue, solid red, and dashed purple lines, respectively. (c) R versus propagation distance s with $\theta = \pi/5$, $2\pi/5$, $3\pi/5$, and $4\pi/5$. (d) Optimum angle $\theta_{\rm opt}$ for the quadrature variance $\langle\hat{X}_\theta^2\rangle$ as a function of the propagation distance s. Panels (a)–(d) are all plotted for $\mathcal{A} = 1$, $\vartheta = 0$, and $g = 1$.

$\hat{a}_1$ [89]:

$$\begin{aligned}\hat{X}_\theta(s) &= \frac{1}{\sqrt{2}}[\hat{a}_1(s)\,e^{-i\theta} + \hat{a}_1^\dagger(s)\,e^{i\theta}] \\ &= \hat{Q}_1(s)\cos\theta + \hat{P}_1(s)\sin\theta,\end{aligned} \tag{31}$$

which satisfies the commutation relation $[\hat{X}_\theta, \hat{X}_{\theta+\frac{\pi}{2}}] = i$. With the results obtained in the last subsection, it is easy to get the expression of the variance of $\hat{X}_\theta$:

$$\langle\hat{X}_\theta^2(s)\rangle = \frac{1}{2}(\mathcal{A}^2 g^2 s\,\cos^2\vartheta\cos\theta + \sin\theta)^2 + \frac{\cos^2\theta}{2}. \tag{32}$$

Shown in Fig. 3(a) is $\langle\hat{X}_\theta^2\rangle$ as a function of $s = z/(2L_{\rm disp})$ and $\theta/(2\pi)$ by taking $\mathcal{A} = 1$, $\vartheta = 0$, and $g = 1$. We see that when $s = 0$, the variance takes the vacuum value $\langle\hat{X}_\theta^2(0)\rangle = 1/2$; for any s, $\langle\hat{X}_{\frac{\pi}{2}}^2(s)\rangle = 1/2$. However, when θ and s are located in the black domains of the figure, the quadrature variance is much smaller than its vacuum value, which means that the SLDS can be significantly quantum-mechanically squeezed. The SLDS can also be made to be antisqueezed, which occurs in the bright domains of the figure.

One can also define the squeezing ratio, i.e., the ratio of the quadrature variance between the value at the position s and that at the position $s = 0$ [33,38], as

$$R = \frac{\langle\hat{X}_\theta^2(s)\rangle}{\langle\hat{X}_\theta^2(0)\rangle}, \tag{33}$$

to characterize the degree of squeezing quantitatively.

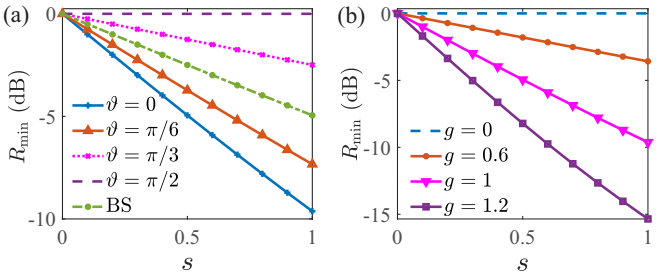

FIG. 4. (a) Minimum squeezing ratio $R_{\min}$ as a function of $s = z/(2L_{\text{disp}})$ and the blackness parameter $\vartheta = 0$, $\pi/3$, $\pi/2$, and $\pi/6$ (with $\mathcal{A} = 1$, $g = 1$). "BS" means the result for the slow-light bright soliton. (b) $R_{\min}$ as a function of s versus the nonlinear coefficients $g = 0$, $g = 0.6$, $g = 1$, and $g = 1.2$ (with $\mathcal{A} = 1$ and $\vartheta = 0$).

Figure 3(b) shows the squeezing ratio R (with unit dB) of the SLDS as a function of angle θ for different propagation distances of $s = 0.3$, 0.6, and 0.9, respectively. We see that the squeezing ratio is sensitive to the selections of θ. Illustrated in Fig. 3(c) is the degree of squeezing (also antisqueezing) in the system, which becomes larger during propagation (i.e., when s increases). However, at some special detection angle (such as $4\pi/5$), the squeezing reaches a threshold. We stress that, in comparison with the quantum squeezing of dark solitons in optical fibers, the quantum squeezing of the SLDS in the present atomic gas is more significant. The typical feature is that the SLDS can acquire a large quantum squeezing in a very short propagation distance (on the order of a centimeter). The physical reason is that the EIT-based atomic gas possesses a larger Kerr nonlinearity (much bigger than that in optical fibers), which makes the typical nonlinearity length L_{nonl} of the system be very small (for the case of the SLDS in the present system, one has $L_{\text{nonl}} \approx L_{\text{disp}} = 0.95$ cm). In addition, the ultraslow propagating velocity of the SLDS is another factor that makes the soliton squeezing more efficient.

By minimizing the quadrature variance $\langle \hat{X}_\theta^2 \rangle$ [Eq. (32)] with respect to θ, we can obtain the optimum angle as a function of the propagation distance s, i.e., $\theta_{\text{opt}} = \theta_{\text{opt}}(s)$, which is plotted in Fig. 3(d). Once $\theta_{\text{opt}}(s)$ is known, experimentally one can choose the optimum detection angle to acquire the largest suppression of the quantum uncertainties in the position and the momentum of the SLDS. With $\theta_{\text{opt}}(s)$ we can get the minimum value of the quadrature as a function of s; meanwhile, the quadrature for the angle $\theta_{\text{opt}} + \pi/2$ will be maximized.

Shown in Fig. 4(a) is the minimum squeezing ratio $R_{\min}$ as a function of $s = z/(2L_{\text{disp}})$ and the blackness parameters $\vartheta = 0$, $\pi/3$, $\pi/2$, and $\pi/6$, for $\mathcal{A} = 1$ and $g = 1$. One sees that (i) $R_{\min}$ is lowered as s is increased, and (ii) $R_{\min}$ is strongly dependent on the parameter ϑ (which characterizes the blackness of the SLDS; see Sec. III A). The darker the SLDS, the larger the minimum squeezing ratio $R_{\min}$. In the figure, the $R_{\min}$ for the slow-light bright soliton is also plotted, given by the dotted dashed green line with circles. We see that if the SLDS is made to be dark enough (i.e., ϑ is small), its minimum squeezing ratio $R_{\min}$ can be much smaller than that of the slow-light bright soliton. This means that the SLDS can have quantum squeezing larger than that of the slow-light bright soliton.

We stress that the minimum squeezing ratio $R_{\min}$ is strongly dependent on the Kerr nonlinearity of the system, which is proportional to the soliton's amplitude. Figure 4(b) shows the result of $R_{\min}$ as a function of s for the nonlinear coefficients $g = 0$, $g = 0.6$, $g = 1$, and $g = 1.2$ (with $\mathcal{A} = 1$ and $\vartheta = 0$). We see that $R_{\min}$ decreases rapidly as g increases. Because the EIT effect can result in a large enhancement of the Kerr nonlinearity and the Kerr nonlinearity can be actively controlled due to the active character of the system (e.g., the nonlinear parameter g can be adjusted by changing the two-photon detuning Δ_2), the EIT-based atomic gas is an excellent platform for realizing large quantum squeezing of the SLDS.

Finally, we indicate that the larger Kerr nonlinearity contributed by the EIT can not only result in the large quantum squeezing of the probe laser pulse (here the SLDS) but also induce an atomic spin squeezing in the system. The result of the atomic spin squeezing in the presence of the SLDS is given in Appendix D.

V. SUMMARY

In this work, we have investigated the quantum effect of the SLDS in a cold atomic gas with defocusing Kerr nonlinearity working on the condition of EIT. We have made an analytical calculation on the quantum fluctuations of the SLDS through solving the BdG equations and the relevant non-Hermitian eigenvalue problem. We found that only a single zero mode is allowed for the quantum fluctuations, which is different from the quantum fluctuations of bright solitons where two independent zero modes occur. We have rigorously proved that the eigenmodes, which consist of continuous modes and the zero mode, are biorthogonal and constitute a complete biorthonormalized basis, which is useful and necessary for the calculation of the quantum fluctuations of the SLDS. We have demonstrated that, due to the large Kerr nonlinearity contributed from the EIT effect, a significant quantum squeezing of the SLDS can be realized; the squeezing efficiency can be manipulated by the Kerr nonlinearity and the blackness and the amplitude of the soliton, which can be much higher than those of the slow-light bright solitons. Our work is useful for developing quantum nonlinear optics and non-Hermitian physics, and for applications in Bose-condensed quantum gases, quantum and nonlinear fiber optics, quantum information processing, and precision measurements, and so on.

ACKNOWLEDGMENT

This work was supported by the National Natural Science Foundation of China under Grant No. 11975098.

APPENDIX A: EXPLICIT EXPRESSIONS OF THE HEISENBERG-LANGEVIN EQUATIONS

Explicit expressions of the Heisenberg-Langevin equation 1(a) are given by

$$i\frac{\partial}{\partial t}\hat{S}_{22} - i\Gamma_{23}\hat{S}_{33} - \Omega_c\hat{S}_{23} + \Omega_c^*\hat{S}_{32} - i\hat{F}_{22} = 0, \tag{A1a}$$

$$i\left(\frac{\partial}{\partial t}+\Gamma_3\right)\hat{S}_{33}+g_p\hat{S}_{13}\hat{E}_p-g_p^*\hat{E}_p^\dagger\hat{S}_{31}+\Omega_c\hat{S}_{23}-\Omega_c^*\hat{S}_{32}-i\hat{F}_{33}=0, \tag{A1b}$$

$$\left(i\frac{\partial}{\partial t}+d_{21}\right)\hat{S}_{21}+\Omega_c^*\hat{S}_{31}-g_p\hat{S}_{23}\hat{E}_p-i\hat{F}_{21}=0, \tag{A1c}$$

$$\left(i\frac{\partial}{\partial t}+d_{31}\right)\hat{S}_{31}+\Omega_c\hat{S}_{21}+g_p(\hat{I}-\hat{S}_{22}-2\hat{S}_{33})\hat{E}_p-i\hat{F}_{31}=0, \tag{A1d}$$

$$\left(i\frac{\partial}{\partial t}+d_{32}\right)\hat{S}_{32}+\Omega_c(\hat{S}_{22}-\hat{S}_{33})+g_p\hat{S}_{12}\hat{E}_p-i\hat{F}_{32}=0. \tag{A1e}$$

Here $\hat{S}_{11}=\hat{I}-\hat{S}_{22}-\hat{S}_{33}$; $\hat{I}$ is the identity operator; and $d_{\alpha\beta}=\Delta_\alpha-\Delta_\beta+i\gamma_{\alpha\beta}$ ($\alpha\neq\beta$), where $\gamma_{\alpha\beta}\equiv(\Gamma_\alpha+\Gamma_\beta)/2+\gamma_{\alpha\beta}^{\rm dep}$, $\Gamma_\beta\equiv\sum_{\alpha<\beta}\Gamma_{\alpha\beta}$, and $\gamma_{\alpha\beta}^{\rm dep}$ is the dephasing rate between $|\alpha\rangle$ and $|\beta\rangle$. $\hat{F}_{\alpha\beta}$ are δ-correlated Langevin noise operators associated with the dissipation in the system, with the two-time correlation function given by

$$\langle\hat{F}_{\alpha\beta}(z,t)\,\hat{F}_{\alpha'\beta'}(z',t')\rangle=\frac{L}{N}\delta(z-z')\delta(t-t')\mathcal{D}_{\alpha\beta,\alpha'\beta'}(z,t), \tag{A2}$$

where $\mathcal{D}_{\alpha\beta,\alpha'\beta'}$ are the atomic diffusion coefficients [90], which can be obtained from the Eqs. (A1) using the generalized fluctuation dissipation theorem. Some of them are given by

$$\mathcal{D}_{21,12}=\Gamma_{23}\langle\hat{S}_{33}\rangle, \tag{A3a}$$

$$\mathcal{D}_{31,13}=0, \tag{A3b}$$

$$\mathcal{D}_{\alpha1,1\beta}=0, \tag{A3c}$$

with $\alpha,\beta=2$ and 3 ($\alpha\neq\beta$).

APPENDIX B: EXPLICIT EXPRESSIONS OF $K(\omega)$, W, AND $\hat{\mathcal{F}}_p(z,t)$

The linear dispersion relation reads

$$K(\omega)=\frac{\omega}{c}+\frac{|g_p|^2N}{c}\frac{\omega+d_{21}}{D(\omega)}. \tag{B1}$$

Here ω is the sideband frequency of the probe pulse. The new noise operator $\hat{\mathcal{F}}_p(z,t)$ is defined by

$$\hat{\mathcal{F}}_p(z,t)=\frac{g_p^*N}{c}\frac{(\omega+d_{21})\hat{F}_{31}(z,t)-\Omega_c\hat{F}_{21}(z,t)}{D(\omega)}, \tag{B2}$$

with $D(\omega)=|\Omega_c|^2-(\omega+d_{21})(\omega+d_{31})$.

By considering the steady-state solution of the Heisenberg-Langevin equations (for which $\hat{S}_{11}=\hat{I}$ and $\hat{S}_{22}=\hat{S}_{33}=0$), we obtain the solution at the first-order approximation, given by

$$\hat{S}_{\alpha1}=a_{\alpha1}^{(1)}g_p\hat{E}_p\ (\alpha=2,3), \tag{B3}$$

and other $\hat{S}_{\alpha\beta}=0$, where

$$a_{\alpha1}^{(1)}=\frac{-\Omega_c^*\delta_{\alpha2}+d_{21}\delta_{\alpha3}}{|\Omega_c|^2-d_{21}d_{31}}. \tag{B4}$$

Proceeding to the next order of iteration by substituting Eq. (B4) into Eqs. (A1), one obtains $\hat{S}_{\alpha\beta}=a_{\alpha\beta}^{(2)}|g_p|^2\hat{E}_p^\dagger\hat{E}_p$ ($\alpha,\beta=1$, 2, and 3). Here

$$a_{11}^{(2)}=\frac{\Gamma_{23}+2D_c}{\Gamma_{13}D_c}2{\rm Im}\big[a_{31}^{(1)*}\big]-\frac{1}{D_c}2{\rm Im}\left[\frac{\Omega_c^*}{d_{32}}a_{21}^{(1)*}\right], \tag{B5a}$$

$$a_{22}^{(2)}=\frac{1}{D_c}2{\rm Im}\left[\frac{\Omega_c^*}{d_{32}}a_{21}^{(1)*}\right]-\frac{\Gamma_{23}+D_c}{\Gamma_{13}D_c}2{\rm Im}\big[a_{31}^{(1)*}\big], \tag{B5b}$$

$$a_{33}^{(2)}=-\frac{1}{\Gamma_{13}}2{\rm Im}\big[a_{31}^{(1)*}\big], \tag{B5c}$$

$$a_{32}^{(2)}=-\frac{1}{d_{32}}\big[a_{21}^{(1)*}+\Omega_c\big(a_{22}^{(2)}-a_{33}^{(2)}\big)\big], \tag{B5d}$$

and other $\hat{S}_{\alpha\beta}=0$, with $D_c=2\gamma_{32}|\Omega_c|^2/|d_{32}|^2$.

Based on the above results, we can proceed to the third-order of iteration. We get

$$\hat{S}_{31}=a_{31}^{(3)}|g_p|^2g_p\hat{E}_p^\dagger\hat{E}_p\hat{E}_p, \tag{B6a}$$

$$a_{31}^{(3)}\equiv\frac{\Omega_ca_{32}^{(2)*}-d_{21}\big[a_{22}^{(2)}+2a_{33}^{(2)}\big]}{|\Omega_c|^2-d_{21}d_{31}}. \tag{B6b}$$

The solutions of other $\hat{S}_{\alpha\beta}$ are also obtained but are omitted here.

The optical susceptibility of the probe field is defined by $\chi_p=\mathcal{N}_a|\mathbf{e}_p\cdot\mathbf{p}_{31}|\,\rho_{31}/(\varepsilon_0\mathcal{E}_p)$, with $\rho_{31}\equiv\langle\hat{S}_{31}\rangle$. Based on the above result, we obtain $\chi_p=\chi_p^{(1)}+\chi_p^{(3)}|\mathcal{E}_p|^2$, with the third-order Kerr nonlinear susceptibility given by

$$\chi_p^{(3)}=\frac{\mathcal{N}_a|\mathbf{p}_{31}|^4}{\varepsilon_0\hbar^3}a_{31}^{(3)}=\frac{2c|\mathbf{e}_p\cdot\mathbf{p}_{31}|^2}{\hbar^2\omega_p}W, \tag{B7a}$$

$$W=\frac{\mathcal{N}_a|\mathbf{e}_p\cdot\mathbf{p}_{31}|^2\omega_p}{2c\varepsilon_0\hbar}a_{31}^{(3)}. \tag{B7b}$$

Generally, $\chi_p^{(3)}$ and W are functions of ω (the sideband frequency of the probe pulse). Since we are interested in the probe-pulse propagation near the center frequency ω_p, the coefficients in the QNLS equation (2) will be estimated at $\omega=0$. In this case, these coefficients are functions of the one- and two-photon detunings (i.e., Δ_3 and Δ_2) and other system parameters.

APPENDIX C: PROOF ON THE COMPLETENESS AND BIORTHONORMALITY OF THE EIGENMODE SET

For investigating the physical properties of the quantum fluctuations of the SLDS, it is necessary to acquire all the eigenmodes of the BdG eigenvalue problem (13). In addition, the eigenmode set obtained should be complete and biorthonormal, which is necessary not only for a complete and correct description of quantum fluctuations of the SLDS but also for obtaining a general and consistent perturbation expansion valid for any perturbation on the soliton when external and/or initial disturbances are applied to the system.

1. Biorthogonality

We first prove the biorthogonality for the continuous modes given by Eqs. (18) and (19). Consider the following integral:

$$\begin{aligned}\langle\Phi_{k'}(\sigma)|\Psi_k(\sigma)\rangle &= \int_{-\infty}^{\infty} d\sigma\,[u_k(\sigma)u_{k'}^*(\sigma) - v_k^*(\sigma)v_{k'}(\sigma)] \\ &= \int_{-\infty}^{\infty} d\sigma\,\frac{e^{i(k-k')\sigma}}{2\pi\sqrt{kk'v(k)v(k')}\mathcal{D}(k)\mathcal{D}(k')}\{A+B\}, \quad \text{(C1)}\end{aligned}$$

with

$$\begin{aligned}A = &\left\{-\tfrac{1}{4}[\mathcal{D}(k')-k']^2+1\right\}\left\{-\tfrac{1}{4}[\mathcal{D}(k)-k]^2+1\right\} \\ &+\left\{-\tfrac{1}{4}[\mathcal{D}(k')+k']^2+1\right\}\left\{\tfrac{1}{4}[\mathcal{D}(k)+k]^2-1\right\} \\ &-2k\mathcal{D}(k')-2k'\mathcal{D}(k), \quad \text{(C2)}\end{aligned}$$

$$\begin{aligned}B = &i\left\{[\mathcal{D}(k)-\mathcal{D}(k')]\left[\tfrac{1}{2}\mathcal{D}(k)\mathcal{D}(k')+kk'+2\right]\right. \\ &\left.+\tfrac{1}{2}[k^2\mathcal{D}(k')-k'^2\mathcal{D}(k)]\right\}\tanh\sigma \\ &+\{(2k'-k)\mathcal{D}(k)+(2k-k')\mathcal{D}(k')\}\,\mathrm{sech}^2\,\sigma \\ &+2i[\mathcal{D}(k')-\mathcal{D}(k)]\tanh\sigma\,\mathrm{sech}^2\,\sigma. \quad \text{(C3)}\end{aligned}$$

It is easy to show that the first term of the right-hand side of Eq. (C1) (related to A) equals $\delta(k-k')$. The second term (related to B) can be calculated by using the following formulas:

$$\int_{-\infty}^{\infty} e^{ikx}\tanh x dx = i\pi\,\mathrm{csch}(\pi k/2), \quad \text{(C4a)}$$

$$\int_{-\infty}^{\infty} e^{ikx}\,\mathrm{sech}^2\,x dx = \pi k\,\mathrm{csch}(\pi k/2), \quad \text{(C4b)}$$

$$\int_{-\infty}^{\infty} e^{ikx}\tanh x\,\mathrm{sech}^2\,x dx = i\pi k^2\mathrm{csch}(\pi k/2)/2. \quad \text{(C4c)}$$

It is also easy to show that the second term equals zero. Thereby, we have

$$\langle\Phi_{k'}(\sigma)|\Psi_k(\sigma)\rangle = \delta(k-k'). \quad \text{(C5)}$$

In a similar way, we can prove the biorthogonality of the zero mode,

$$\langle\Phi_1(\sigma)|\Psi_1(\sigma)\rangle = 1, \quad \text{(C6)}$$

as well as the biorthogonality between the zero mode and the continuous modes,

$$\langle\Phi_1(\sigma)|\Psi_k(\sigma)\rangle = 0. \quad \text{(C7)}$$

2. Completeness

To prove the completeness of the eigenmodes, we consider the expression $|\Phi_1(\sigma)\rangle\langle\Psi_1(\sigma')| + \int_{-\infty}^{+\infty} dk|\Phi_k(\sigma)\rangle\langle\Psi_k(\sigma')|$. Using the results (18)–(22), we have

$$\begin{aligned}&|\Phi_1(\sigma)\rangle\langle\Psi_1(\sigma')| + \int_{-\infty}^{+\infty} dk|\Phi_k(\sigma)\rangle\langle\Psi_k(\sigma')| \\ &= \begin{pmatrix}\mathcal{G}(\sigma) & \mathcal{R}(\sigma)\\ \mathcal{R}(\sigma') & \mathcal{G}(\sigma')\end{pmatrix}. \quad \text{(C8)}\end{aligned}$$

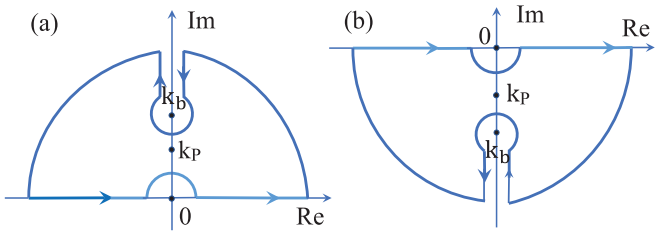

FIG. 5. (a) Integral path of $P(k)$ for $\sigma-\sigma'>0$, with $k_P=2i$ and $k_b=2i\sqrt{1+\gamma^2}$. (b) The same as panel (a) but for $\sigma-\sigma'<0$, with $k_P=-2i$ and $k_b=-2i\sqrt{1+\gamma^2}$. Here Re and Im are the real and imaginary part of complex k, respectively.

Here $\mathcal{G}(\sigma)=X(k)+\psi_1(\sigma)\phi_1^*(\sigma')+\psi_1^*(\sigma)\phi_1(\sigma')$ and $\mathcal{R}(\sigma)=Y(k)+\psi_1(\sigma)\phi_1(\sigma')-\phi_1(\sigma)\psi_1(\sigma')$; $X(k)$ and $Y(k)$ are given by

$$X(k) = \int_{-\infty}^{+\infty}[u_k(\sigma)u_k^*(\sigma') - v_k^*(\sigma)v_k(\sigma')]dk, \quad \text{(C9a)}$$

$$Y(k) = \int_{-\infty}^{+\infty}[u_k(\sigma)v_k^*(\sigma') - v_k^*(\sigma)u_k(\sigma')]dk. \quad \text{(C9b)}$$

Functions $X(k)$ and $Y(k)$ have the following properties: (i) As $k\to\infty$, $X(k)\to\delta(\sigma-\sigma')$ and $Y(k)\to 0$; and (ii) $X(k)$ and $Y(k)$ are analytic in the complex k plane, except for the existence of a single pole at $k=0$, two second-order poles at $k=k_P=\pm 2i$, and two branch points at $k=k_b=\pm 2i\sqrt{1+\gamma^2}$. For convenience, we introduce $P(k)\equiv X(k)-\delta(\sigma-\sigma')$. According to Jordan's lemma, we can use the residue theorem to calculate the integrals in Eqs. (C9a) and (C9b), with the integral path shown in Fig. 5.

After a detailed calculation, we obtain (with $\mathrm{Res}[P(k_s)]$ representing the residue of $P(k)$ at $k=k_s$)

$$\begin{aligned}P(k) &= \begin{cases}2\pi i\mathrm{Res}[P(2i)]+\pi i\mathrm{Res}[P(0)], & \text{for } \sigma-\sigma'>0,\\ -2\pi i\mathrm{Res}[P(-2i)]-\pi i\mathrm{Res}[P(0)], & \text{for } \sigma-\sigma'<0,\end{cases} \\ &= -\frac{1}{2}\mathrm{sech}^2\sigma(-i\gamma\tan\sigma' - i\gamma\sigma'\mathrm{sech}^2\sigma'+1) \\ &\quad -\frac{1}{2}\mathrm{sech}^2\sigma'(i\gamma\tan\sigma + i\gamma\sigma\,\mathrm{sech}^2\sigma+1) \\ &= -\psi_1(\sigma)\phi_1^*(\sigma') - \psi_1^*(\sigma)\phi_1(\sigma'), \quad \text{(C10a)}\\ Y(k) &= -\frac{1}{2}\mathrm{sech}^2\sigma(i\gamma\tan\sigma' + i\gamma\sigma'\mathrm{sech}^2\sigma'+1) \\ &\quad +\frac{1}{2}\mathrm{sech}^2\sigma'(i\gamma\tan\sigma + i\gamma\sigma\,\mathrm{sech}^2\sigma+1) \\ &= -\psi_1(\sigma)\phi_1(\sigma') + \phi_1(\sigma)\psi_1(\sigma'), \quad \text{(C10b)}\end{aligned}$$

which means $\mathcal{G}(\sigma)=\delta(\sigma-\sigma')$ and $\mathcal{R}(\sigma)=0$. Therefore, we obtain

$$\begin{aligned}&|\Phi_1(\sigma)\rangle\langle\Psi_1(\sigma')| + \int_{-\infty}^{+\infty} dk|\Phi_k(\sigma)\rangle\langle\Psi_k(\sigma')| \\ &= I\,\delta(\sigma-\sigma'), \quad \text{(C11)}\end{aligned}$$

which is Eq. (17) given in the main text for $n=1$.

APPENDIX D: ATOMIC SPIN SQUEEZING

The Kerr nonlinearity can not only result in the quantum squeezing of the SLDS but also can cause atomic spin squeezing in the system. To show this, we consider the atomic spin operators [86–88] $\hat{s}_x = \frac{1}{2}(\hat{\sigma}_{12} + \hat{\sigma}_{21})$, $\hat{s}_y = \frac{1}{2i}(\hat{\sigma}_{12} - \hat{\sigma}_{21})$, and $\hat{s}_z = \frac{1}{2}(\hat{\sigma}_{11} - \hat{\sigma}_{22})$, which satisfy the commutation relation $[\hat{s}_l, \hat{s}_m] = i\epsilon_{lmn}\hat{s}_j$. We introduce the quadrature spin operator to calculate the spin squeezing

$$\begin{aligned}\hat{s}_\theta &= \tfrac{1}{2}[\hat{\sigma}_{12}e^{-i\theta} + \hat{\sigma}_{21}e^{i\theta}] \\ &= \cos\theta\,\hat{s}_x + \sin\theta\,\hat{s}_y, \end{aligned} \tag{D1}$$

and define the minimum spin squeezing degree

$$\xi^2 = \min_\theta\left(\frac{\langle\hat{s}_\theta^2\rangle - \langle\hat{s}_\theta\rangle^2}{\langle\hat{s}_z\rangle/2}\right). \tag{D2}$$

From the result given by Eq. (B3) and the relation between $\hat{S}_{\alpha\beta}$ and $\hat{\sigma}_{\alpha\beta}$, we can calculate the minimum spin squeezing degree ξ^2. Shown in Fig. 6 is the result of ξ^2 as a function of the propagation distance s. We see that the system indeed supports atomic spin squeezing, which is also contributed from the Kerr nonlinearity.

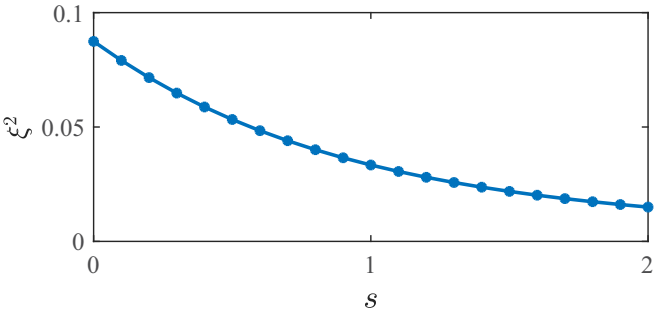

FIG. 6. Minimum atomic spin squeezing degree ξ^2 as a function of propagation distance s.

[1] G. P. Agrawal, *Nonlinear Fiber Optics*, 6th ed. (Academic, New York, 2019).

[2] Y. S. Kivshar and G. P. Agrawal, *Optical Solitons: From Fibers to Photonic Crystals* (Academic, London, 2006).

[3] D. Krökel, N. J. Halas, G. Giuliani, and D. Grischkowsky, Dark-Pulse Propagation in Optical Fibers, Phys. Rev. Lett. **60**, 29 (1988).

[4] S. A. Gredeskul, Y. S. Kivshar, and M. V. Yanovskaya, Dark-pulse solitons in nonlinear-optical fibers, Phys. Rev. A **41**, 3994 (1990).

[5] D. Meshulach and Y. Silberberg, Coherent quantum control of two-photon transitions by a femtosecond laser pulse, Nature (London) **396**, 239 (1998).

[6] W.-H. Cao, S. Li, and K.-T. Chan, Generation of dark pulse trains from continuous-wave light using cross-phase modulation in optical fibers, Appl. Phys. Lett. **74**, 510 (1999).

[7] R. W. Schoenlein, S. Chattopadhyay, H. H. W. Chong, T. E. Glover, P. A. Heimann, C. V. Shank, A. A. Zholents, and M. S. Zolotorev, Generation of femtosecond pulses of synchrotron radiation, Science **287**, 2237 (2000).

[8] D. Farina and S. V. Bulanov, Slow electromagnetic solitons in electron-ion plasmas, Plasma Phys. Rep. **27**, 641 (2001).

[9] X. Xue, Y. Xuan, Y. Liu, P.-H. Wang, S. Chen, J. Wang, D. E. Leaird, M. Qi, and A. M. Weiner, Mode-locked dark pulse Kerr combs in normal-dispersion microresonators, Nat. Photonics **9**, 594 (2015).

[10] N. Bouldja, A. Grabar, M. Sciamanna, and D. Wolfersberger, Slow light of dark pulses in a photorefractive crystal, Phys. Rev. Research **2**, 032022(R) (2020).

[11] M. Fleischhauer, A. Imamoglu, and J. P. Marangos, Electromagnetically induced transparency: Optics in coherent media, Rev. Mod. Phys. **77**, 633 (2005).

[12] K. B. Khurgin and R. S. Tucker (Editors), *Slow Light: Science and Applications* (CRC, Boca Raton, FL, 2009).

[13] Y. Wu and L. Deng, Ultraslow Optical Solitons in a Cold Four-State Medium, Phys. Rev. Lett. **93**, 143904 (2004)

[14] G. Huang, L. Deng, and M. G. Payne, Dynamics of ultraslow optical solitons in a cold three-state atomic system, Phys. Rev. E **72**, 016617 (2005).

[15] Y. Wu and L. Deng, Ultraslow bright and dark optical solitons in a cold three-state medium, Opt. Lett. **29**, 2064 (2004).

[16] C. Hang, G. Huang, and L. Deng, Generalized nonlinear Schrödinger equation and ultraslow optical solitons in a cold four-state atomic system, Phys. Rev. E **73**, 036607 (2006).

[17] H. Michinel, M. J. Paz-Alonso, and V. M. Pérez-García, Turning Light into a Liquid via Atomic Coherence, Phys. Rev. Lett. **96**, 023903 (2006).

[18] Y. Qi, F. Zhou, T. Huang, Y. Niu, and S. Gong, Spatial vector solitons in a four-level tripod-type atomic system, Phys. Rev. A **84**, 023814 (2011).

[19] U. Khadka, J. Sheng, and M. Xiao, Spatial Domain Interactions between Ultraweak Optical Beams, Phys. Rev. Lett. **111**, 223601 (2013).

[20] M. Facão, S. Rodrigues, and M. I. Carvalho Temporal dissipative solitons in a three-level atomic medium confined in a photonic-band-gap fiber, Phys. Rev. A **91**, 013828 (2015).

[21] Z. Bai, W. Li, and G. Huang, Stable single light bullets and vortices and their active control in cold Rydberg gases, Optica **6**, 309 (2019).

[22] Z. Bai, C. Hang, and G. Huang, Storage and retrieval of ultraslow optical solitons in coherent atomic system, Chin. Opt. Lett. **11**, 012701 (2013).

[23] Y. Chen, Z. Bai, and G. Huang, Ultraslow optical solitons and their storage and retrieval in an ultracold ladder-type atomic system, Phys. Rev. A **89**, 023835 (2014).

[24] C. Shou and G. Huang, Storage and retrieval of slow-light dark solitons, Opt. Lett. **45**, 6787 (2020).

[25] V. V. Konotop, J. Yang, and D. A. Zezyulin, Nonlinear waves in PT-symmetric systems, Rev. Mod. Phys. **88**, 035002 (2016).

[26] R. El-Ganainy, K. G. Makris, M. Khajavikhan, Z. H. Musslimani, S. Rotter, and D. N. Christodoulides, Non-Hermitian physics and PT symmetry, Nat. Phys. **14**, 11 (2018).

[27] Y. Ashida, Z. Gong, and M. Ueda, Non-Hermitian physics, Adv. Phys. **69**, 249 (2020).

[28] E. J. Bergholtz, J. C. Budich, and F. K. Kunst, Exceptional topology of non-Hermitian systems, Rev. Mod. Phys. **93**, 015005 (2021).

[29] S. J. Carter, P. D. Drummond, M. D. Reid, and R. M. Shelby, Squeezing of Quantum Solitons, Phys. Rev. Lett. **58**, 1841 (1987).

[30] M. J. Potasek and B. Yurke, Dissipative effects on squeezed light generated in systems governed by the nonlinear Schrodinger equation, Phys. Rev. A **38**, 1335 (1988).

[31] Y. Lai and H. A. Haus, Quantum theory of solitons in optical fibers. I. Time-dependent Hartree approximation, Phys. Rev. A **40**, 844 (1989).

[32] Y. Lai and H. A. Haus, Quantum theory of solitons in optical fibers. II. Exact solution, Phys. Rev. A **40**, 854 (1989).

[33] H. A. Haus and Y. Lai, Quantum theory of soliton squeezing: a linearized approach, J. Opt. Soc. Am. B **7**, 386 (1990).

[34] D. Rand, K. Steiglitz, and P. R. Prucnal, Quantum phase noise reduction in soliton collisions and application to nondemolition measurements, Phys. Rev. A **72**, 041805(R) (2005).

[35] D. Rand, K. Steiglitz, and P. R. Prucnal, Quantum theory of Manakov solitons, Phys. Rev. A **71**, 053805 (2005).

[36] C.-P. Yeang, Quantum theory of a second-order soliton based on a linearization approximation, J. Opt. Soc. Am. B **16**, 1269 (1999).

[37] H. A. Haus and C. X. Yu, Soliton squeezing and the continuum, J. Opt. Soc. Am. B **17**, 618 (2000).

[38] Y. Lai, Quantum theory of soliton propagation: a unified approach based on the linearization approximation, J. Opt. Soc. Am. B **10**, 475 (1993).

[39] Y. Lai and S.-S. Yu, General quantum theory of nonlinear optical-pulse propagation, Phys. Rev. A **51**, 817 (1995).

[40] J. F. Corney and P. D. Drummond, Quantum noise in optical fibers. II. Raman jitter in soliton communications, J. Opt. Soc. Am. B **18**, 153 (2001).

[41] M. Rosenbluh and R. M. Shelby, Squeezed Optical Solitons, Phys. Rev. Lett. **66**, 153 (1991).

[42] P. D. Drummond, R. M. Shelby, S. R. Friberg, and Y. Yamamoto, Quantum solitons in optical fibres, Nature (London) **365**, 307 (1993).

[43] L.-M. Duan and G.-G. Guo, Definition and construction of the quantum soliton states in optical fibers, Phys. Rev. A **52**, 874 (1995).

[44] D. Yao, Quantum fluctuations of optical solitons in fibers, Phys. Rev. A **52**, 4871 (1995).

[45] P. L. Hagelstein, Application of a photon configuration-space model to soliton propagation in a fiber, Phys. Rev. A **54**, 2426 (1996).

[46] M. Margalit and H. A. Haus, Accounting for the continuum in analysis of squeezing with solitons, J. Opt. Soc. Am. B **15**, 1387 (1998).

[47] A. B. Matsko and V. V. Kozlov, Second-quantized models for optical solitons in nonlinear fibers: Equal-time versus equal-space commutation relations, Phys. Rev. A **62**, 033811 (2000).

[48] P. D. Drummond and J. F. Corney, Quantum noise in optical fibers. I. Stochastic equations, J. Opt. Soc. Am. B **18**, 139 (2001).

[49] M. Fiorentino, J. E. Sharping, P. Kumar, A. Porzio, and R. S. Windeler, Soliton squeezing in microstructure fiber, Opt. Lett. **27**, 649 (2002).

[50] V. V. Kozlov and D. A. Ivanov, Accurate quantum nondemolition measurements of optical solitons, Phys. Rev. A **65**, 023812 (2002).

[51] R.-K. Lee, Y. Lai, and B. A. Malomed, Quantum correlations in bound-soliton pairs and trains in fiber lasers, Phys. Rev. A **70**, 063817 (2004).

[52] J. F. Corney, P. D. Drummond, J. Heersink, V. Josse, G. Leuchs, and U. L. Andersen, Many-Body Quantum Dynamics of Polarization Squeezing in Optical Fibers, Phys. Rev. Lett. **97**, 023606 (2006).

[53] M. Tsang, Quantum Temporal Correlations and Entanglement via Adiabatic Control of Vector Solitons, Phys. Rev. Lett. **97**, 023902 (2006).

[54] Y. Lai and R.-K. Lee, Entangled Quantum Nonlinear Schrödinger Solitons, Phys. Rev. Lett. **103**, 013902 (2009).

[55] T. X. Tran, K. N. Cassemiro, C. Söller, K. J. Blow, and F. Biancalana, Hybrid squeezing of solitonic resonant radiation in photonic crystal fibers, Phys. Rev. A **84**, 013824 (2011).

[56] G. R. Honarasa, M. Hatami, and M. K. Tavassoly, Quantum squeezing of dark solitons in optical fibers, Commun. Theor. Phys. **56**, 322 (2011).

[57] P. D. Drummond and M. Hillery, *The Quantum Theory of Nonlinear Optics* (Cambridge University, Cambridge, England, 2014).

[58] A. Hosaka, T. Kawamori, and F. Kannari, Multimode quantum theory of nonlinear propagation in optical fibers, Phys. Rev. A **94**, 053833 (2016).

[59] D. Zou, Z. Li, P. Qin, Y. Song, and M. Hu, Quantum limited timing jitter of soliton molecules in a mode-locked fiber laser, Opt. Express **29**, 34590 (2021).

[60] Finding a complete and orthommormal set of eigenmodes (consisting of zero modes and continuous modes) for the eigenvalue problem of the soliton perturbation is important for implementing perturbation calculations, because such an eigenmode set provides a complete basis that can express (expand) any perturbation to the soliton in the system.

[61] N. Bilas and N. Pavloff, Dark soliton past a finite-size obstacle, Phys. Rev. A **72**, 033618 (2005).

[62] J.-L. Yu, C.-N. Yang, H. Cai, and N.-N. Huang, Direct perturbation theory for the dark soliton solution to the nonlinear Schrödinger equation with normal dispersion, Phys. Rev. E **75**, 046604 (2007).

[63] A. G. Sykes, Exact solutions to the four Goldstone modes around a dark soliton of the nonlinear Schrödinger equation, J. Phys. A: Math. Theor. **44**, 135206 (2011).

[64] P. B. Walczak and J. R. Anglin, Back-reaction of perturbation wave packets on gray solitons, Phys. Rev. A **86**, 013611 (2012).

[65] J. Takahashi, Y. Nakamura, and Y. Yamanaka, Interacting multiple zero mode formulation and its application to a system consisting of a dark soliton in a condensate, Phys. Rev. A **92**, 023627 (2015).

[66] J. Zhu, Q. Zhang, and G. Huang, Quantum squeezing of slow-light solitons, Phys. Rev. A **103**, 063512 (2021).

[67] D. A. Steck, Rubidium 87 D Line Data, http://steck.us/alkalidata/

[68] P.-É. Larré and I. Carusotto, Propagation of a quantum fluid of light in a cavityless nonlinear optical medium: General theory

and response to quantum quenches, Phys. Rev. A **92**, 043802 (2015).

[69] P.-É. Larré and I. Carusotto, Prethermalization in a quenched one-dimensional quantum fluid of light, Eur. Phys. J. D **70**, 45 (2016).

[70] M. J. Gullans, J. D. Thompson, Y. Wang, Q.-Y. Liang, V. Vuletić, M. D. Lukin, and A. V. Gorshkov, Effective Field Theory for Rydberg Polaritons, Phys. Rev. Lett. **117**, 113601 (2016).

[71] If taking $R_0 = 100\mu$m (the transverse radius of the probe field), one has the single-photon half Rabi frequency $g_p = 1.14 \times 10^6 \mathrm{s}^{-1}$. By the requirement $L_{\mathrm{disp}} = L_{\mathrm{nln}} \approx 0.95\,\mathrm{cm}$ (i.e., $g \approx 1$) for forming the soliton, we obtain $n_0 = 9.89 \times 10^3 \gg 1$ using the system parameters indicated in the text.

[72] A. V. Gorshkov, A. André, M. D. Lukin, and A. S. Sørensen, Photon storage in Λ-type optically dense atomic media. I. Cavity model, Phys. Rev. A **76**, 033804 (2007).

[73] A. V. Gorshkov, A. André, M. D. Lukin, and A. S. Sørensen, Photon storage in Λ-type optically dense atomic media. II. Free-space model, Phys. Rev. A **76**, 033805 (2007).

[74] F. H. M. Faisal and J. V. Moloney, Time-dependent theory of non-Hermitian Schrödinger equation: application to multiphoton-induced ionisation decay of atoms, J. Phys. B: At. Mol. Phys. **14**, 3603 (1981).

[75] S.-Y. Lee, Decaying and growing eigenmodes in open quantum systems: Biorthogonality and the Petermann factor, Phys. Rev. A **80**, 042104 (2009).

[76] D. C. Brody, Biorthogonal quantum mechanics, J. Phys. A: Math. Theor. **47**, 035305 (2014).

[77] X.-J. Chen, Z.-D. Chen, and N.-N. Huang, A direct perturbation theory for dark solitons based on a complete set of the squared Jost solutions, J. Phys. A: Math. Gen. **31**, 6929 (1998).

[78] S.-M. Ao and J.-R. Yan, A perturbation method for dark solitons based on a complete set of the squared Jost solutions, J. Phys. A: Math. Gen. **38**, 2399 (2005).

[79] H. Yu and J. Yan, Direct approach to study of soliton perturbations of defocusing nonlinear Schrödinger equation, Commun. Theor. Phys. **42**, 895 (2004).

[80] G. Huang and N. Compagnon, Complete and orthonormal eigenfunctions of excitations to a one-dimensional dark soliton, Phys. Lett. A **372**, 321 (2008).

[81] Here we consider the system with a large size (thermodynamic limit), and there is no external potential. Thus, the Goldstone modes, if they exist, are phononlike continuous modes.

[82] R. Rajaraman, *Solitons and Instantons: An Introduction to Solitons and Instantons in Quantum Field Theory* (North-Holland, Amsterdam, 1987).

[83] J. Yan, Y. Tang, G. Zhou, and Z. Chen, Direct approach to the study of soliton perturbations of the nonlinear Schrödinger equation and the sine-Gordon equation, Phys. Rev. E **58**, 1064 (1998).

[84] G. Huang, L. Deng, J. Yan, and B. Hu, Quantum depletion of a soliton condensate, Phys. Lett. A **357**, 150 (2006).

[85] A. H. Nayeh, *Perturbation Methods* (Wiley, New York, 1973).

[86] J. Ma, X. Wang, C. P. Sun, and F. Nori, Quantum spin squeezing, Phys. Rep. **509**, 89 (2011).

[87] U. L. Andersen, T. Gehring, C. Marquardt, and G. Leuchs, 30 years of squeezed light generation, Phys. Scr. **91**, 053001 (2016).

[88] R. Schnabel, Squeezed states of light and their applications in laser interferometers, Phys. Rep. **684**, 1 (2017).

[89] L. Mandel and E. Wolf, *Optical Coherence and Quantum Optics* (Cambridge University, Cambridge, England, 1995), Chap. 21.

[90] P. Kolchin, Electromagnetically-induced-transparency-based paired photon generation, Phys. Rev. A **75**, 033814 (2007).